


## RESEARCH ARTICLE

WILEY

# Comparison of *in vitro* and *in vivo* models for the elucidation of metabolic patterns of 7-azaindole-derived synthetic cannabinoids exemplified using cumyl-5F-P7AICA

Nadja Walle<sup>1</sup> | Frederike Nordmeier<sup>1</sup> | Adrian A. Doerr<sup>1</sup> | Benjamin Peters<sup>1</sup> |  
Matthias W. Laschke<sup>2</sup> | Michael D. Menger<sup>2</sup> | Peter H. Schmidt<sup>1</sup> |  
Markus R. Meyer<sup>3</sup> | Nadine Schaefer<sup>1</sup> 

<sup>1</sup>Institute of Legal Medicine, Saarland University, Homburg, Germany

<sup>2</sup>Institute for Clinical and Experimental Surgery, Saarland University, Homburg, Germany

<sup>3</sup>Department of Experimental and Clinical Toxicology, Center for Molecular Signaling (PZMS), Saarland University, Homburg, Germany

## Correspondence

Nadine Schaefer, Institute of Legal Medicine, Saarland University, Building 49.1, 66421 Homburg, Germany.  
Email: nadine.schaefer@uks.eu

## Abstract

Due to the dynamic market involving synthetic cannabinoids (SCs), the determination of analytical targets is challenging in clinical and forensic toxicology. SCs usually undergo extensive metabolism, and therefore their main metabolites must be identified for the detection in biological matrices, particularly in urine. Controlled human studies are usually not possible for ethical reasons; thus, alternative models must be used. The aim of this work was to predict the *in vitro* and *in vivo* metabolic patterns of 7-azaindole-derived SCs using 1-(5-fluoropentyl)-*N*-(2-phenylpropan-2-yl)-1*H*-pyrrolo[2,3-*b*]pyridin-3-carboxamide (cumyl-5F-P7AICA) as an example. Different *in vitro* (pooled human liver S9 fraction, pooled human liver microsomes, and pig liver microsomes) and *in vivo* (rat and pig) systems were compared. Monooxygenase isoenzymes responsible for the most abundant phase I steps, namely oxidative defluorination (OF) followed by carboxylation, monohydroxylation, and ketone formation, were identified. In both *in vivo* models, OF/carboxylation and *N*-dealkylation/monohydroxylation/sulfation could be detected. Regarding pHS9 and pig urine, monohydroxylation/sulfation or glucuronidation was also abundant. Furthermore, the parent compound could still be detected in all models. Initial monooxygenase activity screening revealed the involvement of CYP2C19, CYP3A4, and CYP3A5. Therefore, in addition to the parent compound, the OF/carboxylated and monohydroxylated (and sulfated or glucuronidated) metabolites can be recommended as urinary targets. In comparison to literature, the pig model predicts best the human metabolic pattern of cumyl-5F-P7AICA. Furthermore, the pig model should be suitable to mirror the time-dependent excretion pattern of parent compounds and metabolites.

This is an open access article under the terms of the Creative Commons Attribution-NonCommercial-NoDerivs License, which permits use and distribution in any medium, provided the original work is properly cited, the use is non-commercial and no modifications or adaptations are made.

© 2020 The Authors. Drug Testing and Analysis published by John Wiley & Sons Ltd

## KEYWORDS

cumyl-5F-P7AICA, pigs, 7-azaindolesynthetic cannabinoidsurinary excretion pattern

## 1 | INTRODUCTION

In the past few years, new psychoactive substances (NPS), especially synthetic cannabinoids (SCs), appeared on the market via the Internet or head shops as a “legal” alternative to  $\Delta^9$ -tetrahydrocannabinol (THC), because they were initially not controlled. In the following years, the number of different SCs on the market increased steadily.<sup>1</sup> According to the published European Drug Report 2018 of the European Monitoring Centre for Drugs and Drug Addiction (EMCDDA), SCs represent the largest group of NPS.<sup>2</sup> In addition to being the legal alternative to common drugs, the easy accessibility, the cheap availability, and the fact that SCs can hardly be detected in toxicological routine screenings are the main consumption motives. As they act as full agonists at cannabinoid receptors (CB1 and CB2),<sup>2–5</sup> compared to THC higher potencies such as psychoactive effects are expected, leading to an increasing number of intoxications, mass intoxications, and even deaths.<sup>1,6–10</sup> Therefore, they gained increased attention in forensic toxicological analytics. Data on the toxicokinetic (TK) and toxicodynamic properties of SCs are necessary for the interpretation of clinical and forensic toxicological results, but for ethical reasons, human studies are often not possible.

One of the so-called new-generation SCs is 1-(5-fluoropentyl)-N-(2-phenylpropan-2-yl)-1H-pyrrolo[2,3-b]pyridin-3-carboxamide (cumyl-5F-P7AICA), first reported in 2015. Since April 2018, cumyl-5F-P7AICA has been subject to the narcotic law in Germany. Concerning its toxicodynamic properties, Asada et al reported that cumyl-5F-P7AICA acts as a nonselective cannabinoid receptor agonist at CB1 and CB2 receptors.<sup>5</sup> Until today, only little is known about the TK property of cumyl-5F-P7AICA.<sup>11–14</sup>

In general, *in vitro* and *in vivo* assays are available for the elucidation of TK properties. As described elsewhere,<sup>15–17</sup> already-established *in vitro* assays are based on pooled human liver microsomes (pHLM) and cytosol, hepatocyte cell cultures, and pig liver microsomes (PLMs) as well as the pooled human liver S9 fraction (pHS9). Staeheli et al first reported on the *in vitro* metabolism of cumyl-5F-P7AICA using pHLM.<sup>13</sup> The benefits of those *in vitro* assays are low cost and easy handling/storage.<sup>17</sup> Nevertheless, the disadvantage of all *in vitro* models is that they act as a static and the only qualitative model. In contrast, *in vivo* models allow one to consider relevant physiological processes of the body.

As far as cumyl-5F-P7AICA is concerned, *in vivo* data regarding major metabolic pathways have already been published using human urine.<sup>11</sup> The interpretation of the findings was limited, because nothing was known about the time of consumption, the dose, and user habits.<sup>11</sup> Therefore, alternative systematic studies under controlled conditions must be performed for better interpretation and assessment of human TK properties. Common *in vivo* systems to determine the metabolic patterns of drugs are the zebrafish larvae,<sup>18</sup> the rat

model after oral administration,<sup>15</sup> the chimeric mouse model after oral administration,<sup>19</sup> and the pig model.<sup>20–22</sup> Zebrafish larvae are a new *in vivo* model to circumvent an animal experiment request up to 120 h post-fertilization. Yet post-mortem studies are not possible. Rats are comparably easy to handle and maintain, but only small volumes of body fluids are available. Due to the transplantation of human hepatocytes, the chimeric mouse model has already proven to be suitable as an alternative animal model for human administration studies.<sup>19</sup> In analogy to the rat model, chimeric mice are also limited by the small amount of body fluids, resulting in a long sample interval of 24 or 48 h. In comparison, the amount of available body fluids and tissues is higher in pigs. Therefore, repeated sampling is possible, enabling the elucidation of metabolic excretion patterns. In addition, pigs have a great similarity to humans in terms of anatomical structure<sup>23,24</sup> and isoenzymes<sup>25,26</sup> as well as physiological properties, and they have already proven to be suitable in TK studies of other SCs as well as synthetic opioids,<sup>16,20–22,27,28</sup> thus justifying the difficult and laborious experimental procedure for research purposes.

To determine which system is best suited and most practicable to investigate new NPS, different assays should be compared. Cumyl-5F-P7AICA was particularly chosen to study the different *in vitro* and *in vivo* metabolism assays, because certain *in vitro* (pHLM<sup>13</sup>) and human<sup>11</sup> metabolism data have already been published and may be compared with our results. Thus, in the present work, the metabolic pattern of cumyl-5F-P7AICA was determined and its targets were identified using different *in vitro* (pHLM, PLM, pHS9 fraction) and *in vivo* (rat/pig) assays. The obtained results were compared with each other as well as with already-published *in vitro* and *in vivo* data.<sup>11,13</sup> In addition, the main enzyme cytochrome P450 isoenzymes (CYP) was identified.

## 2 | MATERIALS AND METHODS

### 2.1 | Chemicals and reagents

Cumyl-5F-P7AICA (purity 99.72%) was provided by the German Federal Criminal Police Office (Wiesbaden, Germany). HPLC-grade ethanol was purchased from Fisher Scientific (Loughborough, United Kingdom). Glucuronidase (EC no. 3.2.1.32)/arylsulfatase (EC no. 3.1.6.1) from *Helix pomatia* L, LC-MS-grade methanol, analytical-grade ammonium formate, LC-MS-grade formic acid, LC-MS-grade acetonitrile, potassium chloride (KCl), ethylenediaminetetraacetic acid disodium salt (Na<sub>2</sub>EDTA), and all other analytical-grade chemicals and reagents were obtained from Merck (Darmstadt, Germany). pHLM from 25 individual donors with 20-mg microsomal protein per milliliter and 330 pmol of total CYP P450 per milligram protein, pHS9 from 30 individual donors with 20-mg protein per milliliter, baculovirus-infected insect cell microsomes (Supersomes)-

containing 1 nmol/mL of human complementary DNA (cDNA)-expressed cytochrome P450 monooxygenases (CYP) CYP1A2, CYP2A6, CYP2B6, CYP2C8, CYP2C9, CYP2C19, CYP2D6, CYP2E1 (2 nmol/mL), CYP3A4, CYP3A5 (2 nmol/mL), or flavin-containing monooxygenase (FMO) 3 (5 mg protein per milliliter) as well as the UGT (uridine diphosphate [UDP]-glucuronosyltransferase) reaction mix solutions A (25 mM UDP-glucuronic acid) and B (250 mM Tris-HCl, 40 mM MgCl<sub>2</sub>, and 0.125 mg/mL of alamethicin) were provided by Corning (Amsterdam, the Netherlands). Nicotinamide adenine dinucleotide phosphate (NADP<sup>+</sup>) was purchased from Biomol (Hamburg, Germany), and superoxide dismutase (SOD), isocitrate, isocitrate dehydrogenase (IDH), dithiothreitol (DTT), reduced glutathione (GSH), acetyl coenzyme A (AcCoA), acetyl carnitine, 3'-phosphoadenosine-5'-phosphosulfate (PAPS), S-(5'-adenosyl)-L-methionine (SAM), and phenylmethylsulfonylfluoride were obtained from Sigma-Aldrich (Taufkirchen, Germany). The Pierce BCA Protein Assay Kit was purchased from ThermoFisher Scientific (Schwerte, Germany).

All enzyme solutions, microsomes, and CYPs were thawed at 37°C. Then they were snap-frozen in liquid nitrogen and stored at -80°C for further analysis.

## 2.2 | Preparation of PLM

For the preparation of PLM, the liver of one drug-free Swabian Hall strain pig, obtained from Emil Faerber GmbH & Co. KG (Zweibrücken, Germany), was used.<sup>16</sup> The liver was stored at -80°C for further analysis. As previously described,<sup>16</sup> 12.5 g of liver was cut into small pieces. After the addition of homogenization buffer (0.154 M KCl, 1 mM Na<sub>2</sub>EDTA) in a ratio of 15%–20% tissue/volume and phenylmethylsulfonylfluoride (10 µg/mL), the liver was homogenized and centrifuged at 10 000g for 15 min. Then, the supernatant was filled in the centrifugation tubes and ultra-centrifuged at 3°C–4°C and 100 000g for 1.15 h. The pellet (microsomes) was resuspended in washing buffer (0.154 M KCl) and centrifuged again at 3°C–4°C and 100 000g for 1.15 h. After the pellet (microsomes) was resuspended in storing buffer (0.154 M KCl, 0.1 mM Na<sub>2</sub>EDTA), the microsomes were aliquoted and stored at -80°C for further analysis.

For the determination of the obtained protein concentration, a Pierce BCA Protein Assay Kit was used. A mixture of reagent A: reagent B (50:1) was mixed with a part of the produced protein solution. After the mixture was shaken and incubated for 30 min at 60°C, the protein concentration was determined by a photometric measurement (540 nm) of the absorption using a bovine serum albumin calibration curve.

## 2.3 | Incubation conditions and sample preparation for identification of phase I and II metabolites using pHS9 fraction

According to the experimental design published by Richter et al.<sup>17</sup> and other published studies,<sup>15,29</sup> 100 U/mL of SOD, 0.1 mM AcCoA, 2.3 mM acetyl carnitine, 2.5 mM isocitrate, 0.8 U/mL of IDH, 0.6 mM NADP<sup>+</sup>, 2.5 mM Mg<sup>2+</sup>, 25 µg/mL of alamethicin (UGT reaction mix solution B) and 90 mM phosphate buffer (pH 7.4) were initially

preincubated for 10 min at 37°C with a final protein concentration of 2 mg/mL of pHS9. Then, 40 µM aqueous PAPS, 1 mM DTT, 2.5 mM UDP-glucuronic acid (UGT reaction mix solution A), 1.2 mM SAM, and 10 mM GSH were added to the previously produced and preincubated solution. To start the reactions, 25 µM cumyl-5F-P7AICA in phosphate buffer (substrate) was added. All concentrations stated earlier are final concentrations. After the solution was incubated for 60 min at 37°C, 60 µL of the mixture was transferred into a reaction tube, and the reaction was stopped by adding 20 µL of ice-cold acetonitrile. The remaining mixture was further incubated for 5 h. The reactions were stopped by adding 30 µL of ice-cold acetonitrile, and the solutions were cooled at -18°C for 30 min and then centrifuged at 14 000 rpm for 2 min. After the supernatant was transferred into autosampler vials, 5 µL of the solution was injected into a liquid chromatography (LC)-high-resolution mass spectrometry (HRMS) system described later, which is based on an Orbitrap. To remove impurities and possibly interfering compounds, additional blank (without pHS9) and control samples (without substrate) were prepared and incubated.

## 2.4 | Incubation conditions and sample preparation for initial CYP activity screening and identification of phase I metabolites using pHLM/PLM

The samples were incubated according to already-published standard incubation conditions, containing 25 µM cumyl-5F-P7AICA (substrate) and 50 pmol/mL of each CYP isoenzyme (CYP1A2, CYP2A6, CYP2B6, CYP2C8, CYP2C9, CYP2C19, CYP2D6, CYP2E1, CYP3A4, or CYP3A5), 0.25 mg protein per milliliter FMO3, or 1 mg protein per milliliter of pHLM or PLM.<sup>16,17,29,30</sup> All incubation mixtures had a final volume of 50 µL and contained 200 U/mL of SOD, the NADP<sup>+</sup> regenerating system (containing 5 mM isocitrate, 0.5 U/mL of IDH, 5 mM Mg<sup>2+</sup>, 1.2 mM NADP<sup>+</sup>), 90 mM phosphate buffer (pH 7.4), and the substrate as well as the respective enzymes. According to the manufacturer's manual, phosphate buffer was replaced with 90 mM Tris buffer (pH 7.4) in incubations with CYP isoenzymes CYP2A6 and CYP2C9. After preincubation for 10 min, the NADP<sup>+</sup> regenerating system was added to start the reactions. All mixtures were incubations at 37°C. After 30 min the incubation was stopped by the addition of 50 µL of ice-cold acetonitrile. Then, the mixtures were centrifuged for 2 min at 14 000 rpm. After 50 µL of the supernatant was transferred into autosampler vials, 5 µL of the solution was injected into an LC-HRMS/MS system. According to the already-described sample preparation using pHS9, additional control samples (without substrate) were prepared and incubated.

## 2.5 | In vivo studies

### 2.5.1 | Rat

As already described elsewhere,<sup>30–32</sup> the experiment was performed using urine samples from one male Wistar rat (Charles River, Sulzfeld,

Germany) for toxicological diagnostic reasons according to German law. First, one blank rat urine sample was collected before drug administration for removing possible interfering compounds. Then, a single dose of 0.6 mg/kg body weight (BW) of cumyl-5F-P7AICA was orally administered in an aqueous suspension via a gastric intubation. The urine sample of the rat was collected separately from feces over a period of 24 h. The animal was housed in a metabolism cage and had water ad libitum. The urine samples were aliquoted and stored at  $-20^{\circ}\text{C}$  for further analysis.

## 2.5.2 | Pig

The *in vivo* experiment was performed in accordance with the German legislation on protection of animals and the National Institutes of Health Guide for the Care and Use of Laboratory Animals (permission number: 44/2019). According to already-published studies,<sup>16,20–22,27</sup> one domestic male pig of the Swabian Hall strain with a BW of 43.2 kg was used. During the housing, the pig had free access to tap water and daily standard chow. For 12 h before the experiment, the animal had free access to water but was kept fasting.

### *Surgical procedures*

The surgical procedures were performed in accordance with previous studies.<sup>16,20–22,27,28</sup> First, the animal received an intramuscular injection of 30 mg/kg BW of ketamine hydrochloride (Ursotamin, Serumwerke Bernburg, Bernburg, Germany), 2.5 mg/kg BW of xylazine hydrochloride (Rompun, Bayer, Leverkusen, Germany), and 1 mg of atropine (Braun, Melsungen, Germany) as premedication. For maintenance of analgesia, 2%–4% of isoflurane (Forene, AbbVie, Ludwigshafen, Germany) was administered through inhalation. During the whole experiment, the animal was mechanically ventilated with a 1:2 v/v mixture of oxygen and air ( $\text{FiO}_2$  of 0.30, Respirator ABV-U, F. Stephan GmbH, Gackebach, Germany) and volume cycled with a tidal volume of 10–12 mL/kg BW. To ensure sufficient fluid replacement with 0.9% of sodium chloride (8 mL/kg/h, Braun), the left ear vein was catheterized. For blood sampling and monitoring of the mean central venous pressure, a triple-lumen 7F (Certofix Trio, Braun) central venous catheter was placed in the jugular vein. In addition, a suprapubic catheter (Cystofix, Braun) was placed in the bladder for collecting urine. Following the aforementioned measures, the animal was then allowed to stabilize for 10–15 min.

### *Study design*

First, 2 mL of a stock solution containing 5 mg/mL of cumyl-5F-P7AICA in ethanol was prepared. To obtain the desired dose of 200  $\mu\text{g}/\text{kg}$  BW, the required volume of the stock solution (1728  $\mu\text{L}$ ) was filled with ethanol (272  $\mu\text{L}$ ) to a volume of 2 mL. Analogous to previous studies,<sup>27,28</sup> the prepared solution was administered within 12 min by nebulization of cumyl-5F-P7AICA applying the inspiration-triggered mode ( $<0.2$  mL/min) of the M-neb flow<sup>+</sup> ventilation ultrasonic nebulizer MN-300/7 (Nebutech, Elsenfeld, Germany). Through the inspiratory limb and the tracheal tube, the aerosol was delivered

into the ventilated lung of the pig. The urine samples were collected hourly ( $t_1 = 0\text{--}1$  h,  $t_2 = 1\text{--}2$  h,  $t_3 = 2\text{--}3$  h,  $t_4 = 3\text{--}4$  h,  $t_5 = 4\text{--}5$  h,  $t_6 = 5\text{--}6$  h,  $t_7 = 6\text{--}7$  h, and  $t_8 = 7\text{--}8$  h) after the beginning of inhalative administration. In addition, one urine sample was collected before administration ( $t_0$ ). All collected urine samples were stored at  $-20^{\circ}\text{C}$  for further analysis.

## 2.6 | Preparation of rat and pig urine samples for identification of phase I and II metabolites

According to published procedures,<sup>15,30,33</sup> phase I and II metabolites in urine samples were identified after protein precipitation with acetonitrile. Therefore, 100  $\mu\text{L}$  of urine was mixed with 500  $\mu\text{L}$  of acetonitrile. After shaking, the mixture was centrifuged for 2 min at 14 000 rpm. The supernatant was transferred into new vials and then evaporated to dryness under a gentle stream of nitrogen at  $60^{\circ}\text{C}$ . Subsequently, the residue was dissolved in 50  $\mu\text{L}$  of a mixture of eluents A and B (1:1, v/v). The composition of the eluents is described in the next section. The solution was transferred into autosampler vials, and 1  $\mu\text{L}$  of the solution was injected into an LC-HRMS/MS system.

## 2.7 | LC-HRMS/MS apparatus

As already described in other studies,<sup>15,16</sup> the extracts were analyzed using a Dionex UltiMate 3000 RS pump consisting of a degaser, a quaternary pump, and an UltiMate autosampler (ThermoFisher Scientific, Dreieich, Germany). The used LC system was coupled to a TF Q-Exactive Plus system equipped with a heated electrospray ionization (HESI)-II source.

The gradient elution of the LC system was performed using a TF Accucore Phenylhexyl column (100  $\times$  2.1 mm, 2.6  $\mu\text{m}$ ), with mobile phases consisting of 2 mM aqueous ammonium formate plus 0.1% (v/v) formic acid and 0.1% (v/v) acetonitrile (pH 3, eluent A) and 2 mM ammonium formate solution with acetonitrile/methanol (50:50, v/v) plus 0.1% (v/v) formic acid and 1% (v/v) water (eluent B). The column oven temperature was set to  $60^{\circ}\text{C}$ . The settings of the gradient and the flow rate of the eluents were as follows: 0–1.0 min 99% A (0.5 mL/min flow rate), 1–10 min to 1% A (0.5 mL/min flow rate), 10–11.5 min hold 1% A (0.8 mL/min flow rate), 11.5–13.5 min hold 99% A (0.8 mL/min flow rate).

The settings for the HESI-II-source were as follows: spray voltage, 3.00 kV; heater temperature,  $320^{\circ}\text{C}$ ; sheath gas, 60 arbitrary units (AU); auxiliary gas, 10 AU; and S-lens RF level, 60.0.

The mass spectrometer was operated in positive-ionization mode with full scan (FS) and a subsequent data-dependent acquisition (DDA) mode. According to the manufacturer's recommendations, mass calibration was done before analysis using external mass calibrators. For FS mode, the following settings were defined: maximum injection time (IT), 120 ms; resolution, 35,000; scan range,  $m/z$  200–650; microscans, 1; and automatic gain control (AGC) target,

**TABLE 1** Identification (ID), cumyl-5F-P7AICA and its metabolites, elemental composition, exact masses, accurate masses, characteristic product ions, mass errors, and retention time (RT) of the compounds detected in pooled human liver microsome, pig liver microsome, pooled human liver S9 fraction incubations, rat urine after oral administration, and pig urine after inhalative administration

ID	Cumyl-5F-P7AICA and its metabolites	Elemental composition	Monoisotopic exact masses	Monoisotopic accurate masses	Accurate fragment masses (m/z)									
					Error (ppm)	Product 1	Error (ppm)	Product 2	Error (ppm)	Product 3	Error (ppm)	Product 4	Error (ppm)	RT (min)
M0	Cumyl-5F-P7AICA	C <sub>22</sub> H <sub>24</sub> O <sub>8</sub> N <sub>3</sub> F	368.2132	368.2129	-0.9399	250.1349	-0.5776	233.1083	-0.8213	145.0395	-0.7159	119.0857	1.7179	7.63
M1	Carboxamide	C <sub>13</sub> H <sub>16</sub> O <sub>8</sub> N <sub>3</sub> F	250.1350	250.1346	-1.8586	233.1082	-1.3450	207.1289	-1.3604	145.0394	-1.3471	119.0604	0.6122	7.63
M1	Oxidative defluorinated (OF) and carboxylated	C <sub>22</sub> H <sub>25</sub> O <sub>8</sub> N <sub>3</sub>	380.1968	380.1965	-0.9613	262.1183	-1.1492	244.1078	-0.9611	201.1021	-0.7871	119.0857	1.6538	6.71
M2	Monohydroxylated <sup>1</sup>	C <sub>22</sub> H <sub>26</sub> O <sub>8</sub> N <sub>3</sub> F	384.2081	384.2075	-1.7238	250.1348	-0.9436	145.0397	0.6518	135.0804	-0.2051	107.0494	2.7750	7.32
M3	Monohydroxylated <sup>2</sup>	C <sub>22</sub> H <sub>26</sub> O <sub>8</sub> N <sub>3</sub> F	384.2081	384.2078	-1.0883	266.1297	-0.8710	145.0396	-0.6107	119.0857	1.6538	91.0547	5.4784	6.71
M4	Ketone	C <sub>22</sub> H <sub>24</sub> O <sub>8</sub> N <sub>3</sub> F	382.1925	382.1915	-2.6255	264.1140	-0.8983	247.0876	-0.5328	221.1081	-1.6940	119.0857	1.5898	7.06
M5	N-Dealkylated	C <sub>17</sub> H <sub>17</sub> O <sub>8</sub> N <sub>3</sub>	280.1444	280.1442	-0.8681	162.0662	-0.1625	119.0606	1.6374	-	-	-	-	6.13
M6	Dihydroxylated <sup>1</sup>	C <sub>22</sub> H <sub>26</sub> O <sub>8</sub> N <sub>3</sub> F	400.2030	400.2030	-0.3098	250.1350	0.0934	233.1084	-0.2322	151.0754	0.4505	123.0443	1.6426	6.53
M7	Dihydroxylated <sup>2</sup>	C <sub>22</sub> H <sub>26</sub> O <sub>8</sub> N <sub>3</sub> F	400.2030	400.2030	-0.1573	282.1247	-0.4281	239.1184	-2.6030	162.0658	-2.5163	119.0858	2.1023	6.32
M8	OF-monohydroxylated <sup>2</sup>	C <sub>22</sub> H <sub>27</sub> O <sub>8</sub> N <sub>3</sub>	382.2125	382.2123	-0.4629	264.1342	-0.4266	203.1181	1.0505	119.0857	1.8460	91.0549	7.8245	6.14
M9	Carboxamide-monohydroxylated <sup>2</sup>	C <sub>13</sub> H <sub>16</sub> O <sub>8</sub> N <sub>3</sub> F	266.1299	266.1298	-0.6417	223.1241	-0.0813	174.0663	0.5500	145.0397	0.1258	119.0606	2.0860	6.79
M10	Monohydroxylated <sup>3</sup>	C <sub>22</sub> H <sub>26</sub> O <sub>8</sub> N <sub>3</sub> F	384.2081	384.2066	-4.1067	266.1301	0.5050	223.1240	-0.5600	161.0346	0.1395	135.0553	0.0625	7.19
M11	N-Dealkylated-monohydroxylated <sup>3</sup>	C <sub>17</sub> H <sub>17</sub> O <sub>8</sub> N <sub>3</sub>	296.1393	296.1383	-3.5378	178.0608	-0.8954	161.0348	1.6556	135.0553	0.2885	-	-	5.38
M12	N-Dealkylated-monohydroxylated <sup>1</sup>	C <sub>17</sub> H <sub>17</sub> O <sub>8</sub> N <sub>3</sub>	296.1393	296.1399	1.8209	162.0658	-2.2338	145.0395	-1.2419	135.0804	-0.5440	119.0604	0.1636	5.04
M13	OF-carboxamide and carboxylated	C <sub>13</sub> H <sub>15</sub> O <sub>8</sub> N <sub>3</sub>	262.1186	262.1183	-1.3821	244.1077	-1.5237	201.1020	-1.2424	145.0395	-1.2419	119.0605	1.2529	6.56
M14	OF-carboxamide	C <sub>13</sub> H <sub>17</sub> O <sub>8</sub> N <sub>3</sub>	248.1393	248.1393	-0.1636	231.1126	-0.7751	205.1335	-0.1977	145.0396	-0.1898	131.0604	0.2650	6.74
M15	OF	C <sub>22</sub> H <sub>27</sub> O <sub>8</sub> N <sub>3</sub>	366.2176	366.2172	-1.1197	248.1391	-0.9015	231.1125	-1.2372	205.1334	-0.5697	119.0857	1.5898	6.73
M16	OF-monohydroxylated <sup>1</sup>	C <sub>22</sub> H <sub>27</sub> O <sub>8</sub> N <sub>3</sub>	382.2125	382.2133	2.0921	248.1394	0.3283	205.1334	-0.5697	135.0805	0.5856	107.0495	3.7728	6.02
M17	Dihydroxylated <sup>1+2</sup>	C <sub>22</sub> H <sub>26</sub> O <sub>8</sub> N <sub>3</sub> F	400.2030	400.2020	3.3504	266.1285	-5.4579	223.1242	0.5341	135.0808	2.5059	107.0500	7.6214	5.88
M18	N-Dealkylated-monohydroxylated <sup>1</sup> and sulfated	C <sub>17</sub> H <sub>17</sub> O <sub>8</sub> N <sub>3</sub> S	376.0961	376.0956	-1.3979	296.1393	-0.0340	162.0659	-1.7630	135.0810	3.9744	119.0605	0.7403	4.86
M19	Monohydroxylated <sup>1</sup> and sulfated	C <sub>22</sub> H <sub>26</sub> O <sub>8</sub> N <sub>3</sub> FS	464.1649	464.1661	2.3275	384.2087	1.4534	250.1354	1.4355	233.1088	1.5352	135.0807	2.0541	6.18
M20	Monohydroxylated <sup>1</sup> and glucuronidated	C <sub>28</sub> H <sub>34</sub> O <sub>8</sub> N <sub>3</sub> F	560.2402	560.2398	-0.8256	384.2081	-0.2940	250.1349	-0.5776	135.0805	0.4726	107.0495	3.1314	6.09
M21	Dihydroxylated <sup>1+2</sup> and sulfated	C <sub>22</sub> H <sub>26</sub> O <sub>8</sub> N <sub>3</sub> FS	480.1599	480.1604	1.0194	400.2032	0.2239	266.1301	0.6197	135.0806	1.0374	119.0609	4.1365	5.62
M22	Dihydroxylated <sup>1+1</sup> and sulfated	C <sub>22</sub> H <sub>26</sub> O <sub>8</sub> N <sub>3</sub> FS	480.1599	480.1607	1.6550	400.2019	-2.9788	250.1350	-0.1506	151.0755	1.0565	123.0443	-0.0936	6.55
M23	N-Dealkylated-monohydroxylated <sup>1</sup> and glucuronidated	C <sub>23</sub> H <sub>25</sub> O <sub>8</sub> N <sub>3</sub>	472.1714	472.1718	0.6602	296.1385	-2.8164	162.0658	-2.5163	135.0800	-3.5940	119.0608	3.6239	4.34
M24	Monohydroxylated <sup>2</sup> and glucuronidated	C <sub>28</sub> H <sub>34</sub> O <sub>8</sub> N <sub>3</sub> F	560.2402	560.2360	-7.5802	384.2092	2.6449	266.1302	1.1931	174.0665	1.9526	119.0860	4.0243	6.43

Note. 1, aryl-monohydroxylated; 2, 5-fluoropentyl-monohydroxylated; 3, 7-azaindole-monohydroxylated.

1e6. The DDA mode was used, with the addition of an inclusion list containing the  $m/z$  values of expected compounds. The following settings were programmed for DDA mode: maximum IT, 250 ms; resolution, 17 500; AGC target,  $2e5$ ; loop count, 5; isolation window, 1.0  $m/z$ ; dynamic exclusion, off; spectrum data type, profile; underfill ratio, 0.5%; option "do not pick others," enabled; microscans, 1; high collision dissociation with stepped normalized collision energy, 17.5%, 35%, and 52.5%. For data handling, TF Xcalibur Qual Browser software version 3.0.63 was used.

### 3 | RESULTS AND DISCUSSION

#### 3.1 | Dosage

A 0.6 mg/kg BW dose was administered orally to the rat. For the study of pigs, a 200  $\mu\text{g}/\text{kg}$  BW dose was inhalatively administered, resulting in a total dose of  $\sim 8.64$  mg. These doses were calculated based on reports of common drug users, recommending a dose of SC in the range of 0.5 – 20 mg, depending on the route of administration.<sup>34</sup> In addition, comparable dosages have already been established in previous studies on NPS.<sup>16,21,22,27,28</sup>

#### 3.2 | General findings

The aim of the study was to identify the *in vitro* and *in vivo* metabolic patterns of cumyl-5F-P7AICA and compare the results with already-published pHLM and human data. In all blank and control samples of the *in vitro* assays as well as in all rat and pig urine specimens collected before drug administration, neither the parent compound nor any metabolite could be found. In all blank samples as well as in pH59-,

pHLM-, and PLM incubations, a compound with a mass of  $m/z$  250.1346 could be detected. The mass difference of  $m/z$  118.0786 to the precursor mass (PM) of the parent compound ( $m/z$  368.2132) indicated a cleavage of the cumyl moiety. The resulting carboxamide M0 (Table 1; Figure S1 [supporting information]) was identified by the product ion (PI) at  $m/z$  233.1082 representing hydrolysis of the amide moiety,  $m/z$  207.1289 indicating the cleavage of the complete amide residue, and the PI at  $m/z$  145.0394 and  $m/z$  119.0604 corresponding to an unaltered 7-azaindole core structure. Therefore, M0 has been identified as an impurity, but interfering substances could be excluded.

Metabolites of cumyl-5F-P7AICA could clearly be identified in all *in vitro* as well as in all *in vivo* assays using LC-HRMS/MS fragmentation. The parent compound (Table 1; Figure 1) could still be observed in all *in vitro* assays and in rat urine, as well as in the early pig urinary samples.

Cumyl-5F-P7AICA (protonated mass, PM of  $m/z$  368.2132, Table 1; Figure 1) was identified by the PI at  $m/z$  233.1083 and  $m/z$  250.1349, indicating a cleavage at the amide moiety. Furthermore, the PI at  $m/z$  145.0395 and  $m/z$  174.0661 represented an unaltered 7-azaindole core structure. The additional presence of  $m/z$  119.0857 has resulted from an unaltered cumyl moiety, whereas  $m/z$  91.0548 exhibited cumyl moiety after the cleavage of the methyl units. The fragmentation pattern of the parent compound is consistent with the findings of Bovens et al.<sup>14</sup>

The respective metabolites were identified by comparison of their  $\text{MS}^2$  spectra with the  $\text{MS}^2$  spectra of the parent compound cumyl-5F-P7AICA. An overview of all tentatively identified phase I and II metabolites using *in vitro* and *in vivo* assays is presented in Table 1. The table includes elemental composition, exact masses, accurate masses, mass error, characteristic fragment ions, and retention time. Due to the high number of metabolites found, not all are discussed in detail in the following section.

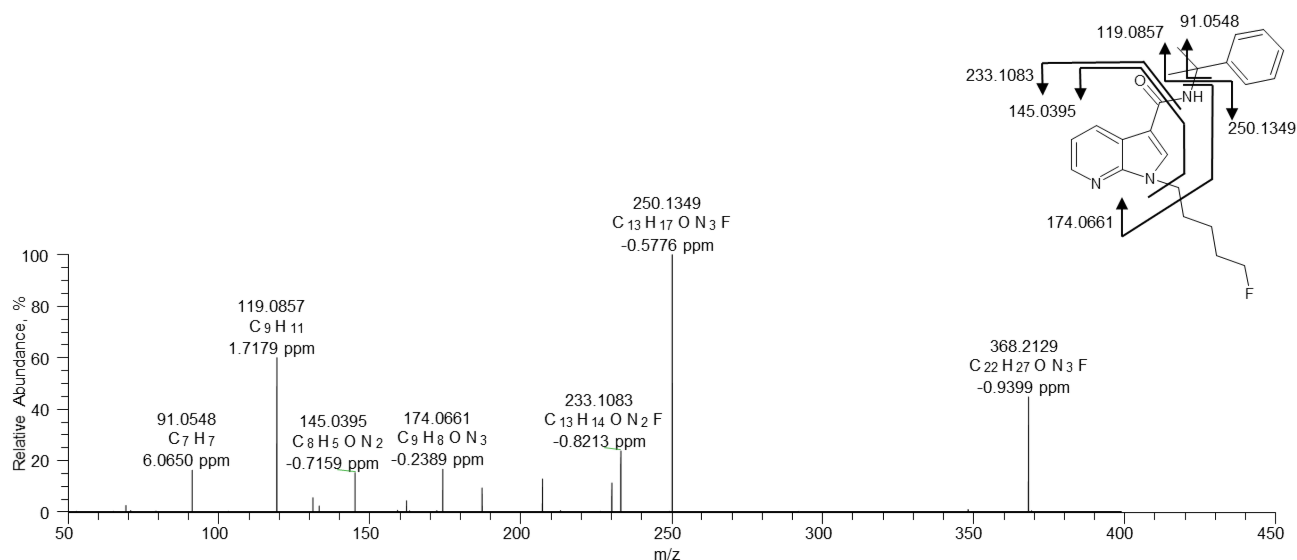


**FIGURE 1** HRMS/MS spectra of cumyl-5F-P7AICA identified in pooled human liver S9 fraction incubation containing 25  $\mu\text{M}$  cumyl-5F-P7AICA [Colour figure can be viewed at [wileyonlinelibrary.com](http://wileyonlinelibrary.com)]



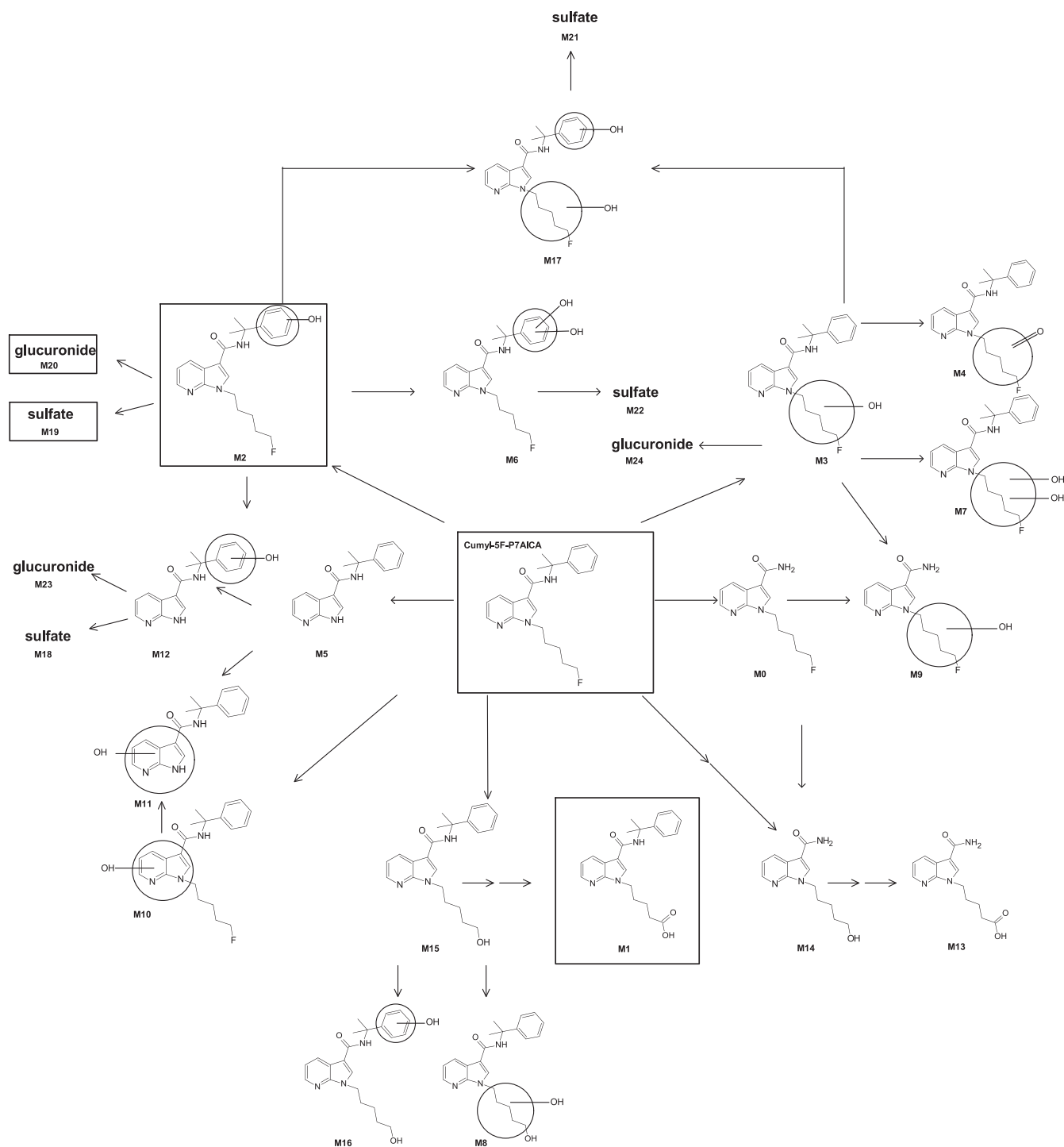


**FIGURE 2** Metabolic patterns of cumyl-5F-P7AICA (M0–M24) elucidated in pooled human liver S9 fraction, pooled human liver microsomes/published data using pHLM,<sup>9</sup> pig liver microsomes, rat urine, pig urine, and/or human urine (HU).<sup>7</sup> Urinary targets are marked in boxes

### 3.3 | LC-HRMS/MS fragmentation and identification of cumyl-5F-P7AICA and its *in vitro* phase I and II metabolites using pHLM, PLM, and pH59

#### 3.3.1 | pHLM/PLM

Eleven phase I metabolites could be detected in pHLM and PLM incubation samples (Figure 2). In addition to the already-described presence of the parent compound, major metabolic pathways of cumyl-5F-P7AICA seemed to be oxidative defluorination (OF) followed by carboxylation, aryl-monohydroxylation, 5-fluoropentyl-monohydroxylation, and ketone formation, as well as *N*-dealkylation in both *in vitro* incubation assays. In addition, aryl-dihydroxylation could be detected in pHLM incubation.

The OF/carboxylated metabolite (M1, PM of  $m/z$  380.1968, Table 1; Figure 3) was identified by the most abundant and characteristic PI at  $m/z$  119.0857 and  $m/z$  262.1183, indicating the cleavage of the cumyl moiety. As already shown in the fragmentation pattern of cumyl-5F-P7AICA, the PI at  $m/z$  91.0548 suggested the cumyl moiety after the cleavage of the methyl units. The unaltered 7-azaindole core structure was identified by the PI at  $m/z$  145.0396. The cleavage of the C–O bond of the carboxyl unit resulted in the PI at  $m/z$  244.1078 and  $m/z$  201.1021, whereas the amide moiety is still present at  $m/z$  244.1078.

The aryl-monohydroxylated metabolite (M2, PM of  $m/z$  384.2081, Table 1; Figure 4A) was identified by the PI at  $m/z$  135.0804 and  $m/z$  107.0494, which can be explained by a mass shift of +16 u of the fragmentation pattern of the unaltered cumyl moiety of cumyl-5F-P7AICA with  $m/z$  119.0857 and  $m/z$  91.0548. The PI at  $m/z$  250.1348 indicated the cleavage of the hydroxylated cumyl moiety. The additional presence of the PI at  $m/z$  145.0397 and  $m/z$  174.0660 resulted from an unaltered 7-azaindole core structure.

In comparison, the 5-fluoropentyl-monohydroxylated metabolite (M3, PM of  $m/z$  384.2081, Table 1; Figure 4B) was identified by the

PI at  $m/z$  266.1297,  $m/z$  119.0857, and  $m/z$  91.0547, indicating the cleavage of the cumyl moiety. The PI at  $m/z$  266.1297 exhibited a hydroxylation at the 5-fluoropentyl or 7-azaindole moiety. The additional presence of the PI at  $m/z$  145.0396 and  $m/z$  174.0661 suggested an unaltered 7-azaindole core structure. Therefore, hydroxylation was formed at the 5-fluoropentyl moiety.

Ketone formation resulting in M4 (PM of  $m/z$  382.1925, Table 1; Figure S2 [supporting information]) was identified by the PI at  $m/z$  264.1140 and  $m/z$  119.0857, indicating the cleavage of the cumyl moiety. Hydrolysis of the amide unit was identified by the PI at  $m/z$  247.0876, whereas  $m/z$  221.1081 exhibited the cleavage of the bond between the amide and the 7-azaindole core.

The *N*-dealkylated metabolite (M5, PM of  $m/z$  280.1444, Table 1; Figure 5A) was identified by the presence of the most abundant and characteristic PI at  $m/z$  162.0662, representing cleavage of the cumyl moiety. The unaltered 7-azaindole core structure formed the PI at  $m/z$  119.0606.

The aryl-dihydroxylated metabolite (M6, PM at  $m/z$  400.2030, Table 1; Figure S3A [supporting information]) was identified by the presence of the PI at  $m/z$  250.1350, which could also be found in HRMS/MS spectra of the aryl-monohydroxylated metabolite, as well as the parent compound, indicating no hydroxylation at the 7-azaindole or 5-fluoropentyl moiety. The cleavage of the dihydroxylated aryl moiety was also characterized by the PI at  $m/z$  151.0754 and  $m/z$  123.0443, which can be explained by a mass shift of +32 u to the PI at  $m/z$  119.0857 and  $m/z$  91.0548 of the unaltered cumyl moiety or +16 u to the PI at  $m/z$  135.0804 and  $m/z$  107.0494 of the aryl-monohydroxylated part.

Furthermore, the 5-fluoropentyl-dihydroxylated metabolite (M7, PM at  $m/z$  400.2030, Table 1; Figure 3B) was identified by the PI at  $m/z$  119.0858, indicating the cleavage of the cumyl moiety. The PI at  $m/z$  282.1247 and  $m/z$  239.1184, indicating the hydroxylation at the 7-azaindole core or 5-fluoropentyl chain, and the additional presence of  $m/z$  162.0658 resulted from an unaltered 7-azaindole core.

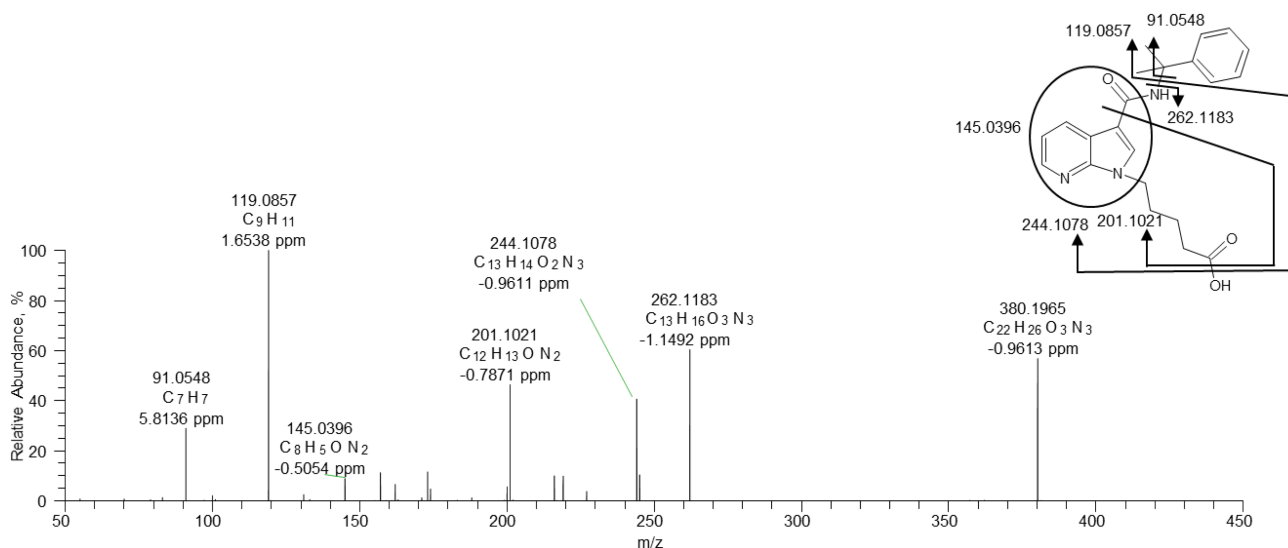


**FIGURE 3** HRMS/MS spectra of the oxidative defluorinated and carboxylated metabolite M1 identified in pooled human liver S9 fraction incubation containing 25  $\mu$ M cumyl-5F-P7AICA [Colour figure can be viewed at [wileyonlinelibrary.com](http://wileyonlinelibrary.com)]



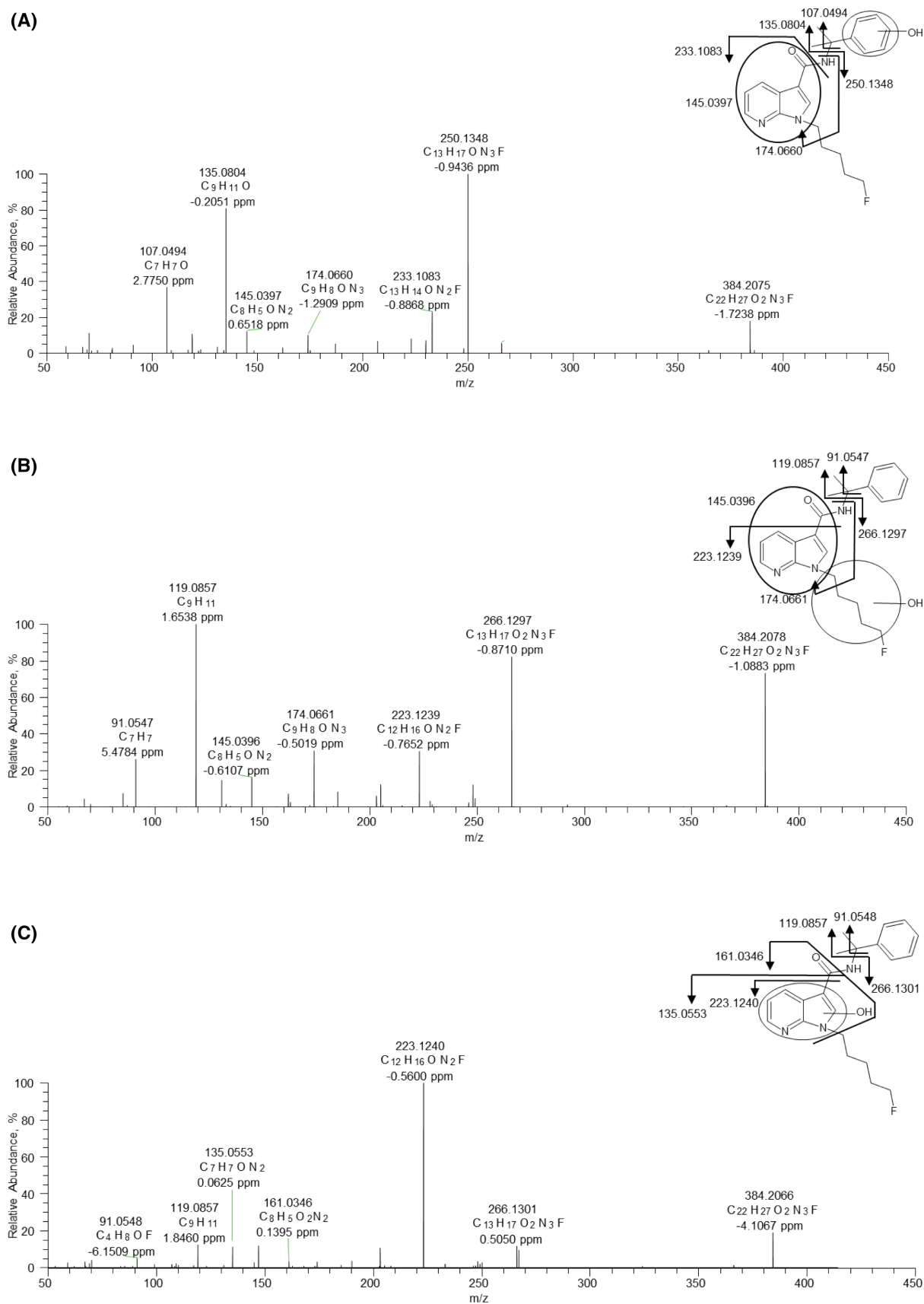


**FIGURE 4** HRMS/MS spectra of A, aryl-monohydroxylated (M2); B, 5-fluoropentyl-monohydroxylated (M3); and C, 7-azaindole-monohydroxylated (M10) metabolites of cumyl-5F-P7AICA identified in pooled human liver S9 fraction incubation containing 25  $\mu$ M cumyl-5F-P7AICA [Colour figure can be viewed at [wileyonlinelibrary.com](http://wileyonlinelibrary.com)]

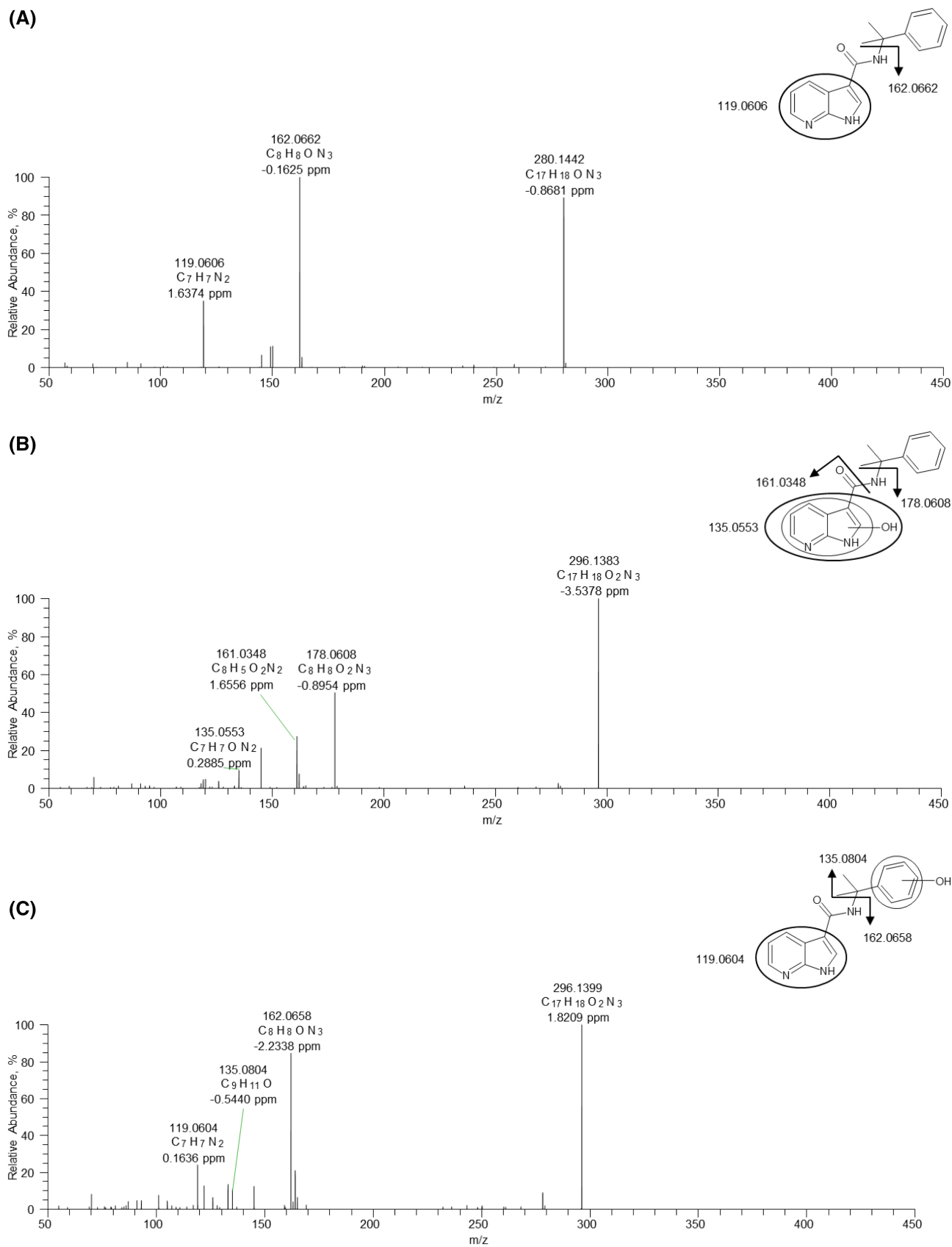


**FIGURE 5** HRMS/MS spectra of A, *N*-dealkylated (M5); B, *N*-dealkylated-7-azaindole-monohydroxylated (M11); and C, *N*-dealkylated-aryl-monohydroxylated (M12) metabolites of cumyl-5F-P7AICA identified in rat urine following a single oral administration of 0.6 mg/kg body weight dose of cumyl-5F-P7AICA [Colour figure can be viewed at [wileyonlinelibrary.com](http://wileyonlinelibrary.com)]

The OF/5-fluoropentyl-monohydroxylated metabolite (M8, PM at  $m/z$  382.2125, Table 1; Figure S4A [supporting information]) was identified by the presence of the PI at  $m/z$  119.0857, representing the cleavage of the cumyl moiety. The PI at  $m/z$  264.1342, indicating the hydroxylation at the 7-azaindole core or 5-fluoropentyl chain, and the additional presence of  $m/z$  174.0666 and  $m/z$  145.0401 represented an unaltered 7-azaindole core.

The carboxamide/5-fluoropentyl-monohydroxylated metabolite (M9, PM at  $m/z$  266.1299, Table 1; Figure S5 [supporting information]), not detected in pHLM, was identified by the presence of the PI at  $m/z$  223.1241, indicating a hydroxylation at the 7-azaindole core or 5-fluoropentyl chain, and the additional presence of  $m/z$  145.0397,  $m/z$  174.0663, and  $m/z$  119.0606 representing an unaltered 7-azaindole core. However, the exact position of the hydroxylation at the aryl or 5-fluoropentyl moiety could not be identified by the methods applied.

### 3.3.2 | pHS9 fraction

As far as pHS9 incubations are concerned, phase II metabolites could be identified in addition to phase I metabolites due to the addition of cofactors. In total, 14 phase I and 6 phase II metabolites were found (Figure 2).

The major metabolic pathways in pHS9 incubation seemed to be those found in pHLM and PLM incubations, extended by mono- and dihydroxylation followed by glucuronidation and sulfation. The metabolites described later could additionally be identified in pHS9 incubation samples.

The 7-azaindole-monohydroxylated metabolite (M10, PM at  $m/z$  384.2081, Table 1; Figure 4C) was identified by the PI at  $m/z$  223.1240 and  $m/z$  266.1301, indicating a hydroxylation at the 7-azaindole core or 5-fluoropentyl chain. The PI at  $m/z$  119.0857 and  $m/z$  91.0548 indicated the cleavage of the unaltered cumyl moiety, and the additional presence of the PI at  $m/z$  135.0553 and  $m/z$  161.0346 represented a hydroxylated 7-azaindole core structure.

Phase II metabolites were mainly formed by glucuronidation or sulfation of the monohydroxylated, dihydroxylated, and *N*-dealkylated/aryl-monohydroxylated compounds. The *N*-dealkylated/aryl-monohydroxylated/sulfated metabolite (M18, PM at  $m/z$  376.0961, Table 1) was identified by the aglycone at  $m/z$  296.1393, as well as the PI at  $m/z$  135.0810 represented by a hydroxylated cumyl unit, and  $m/z$  162.0659 indicated an unaltered 7-azaindole core structure.

The aryl-monohydroxylated/sulfated metabolite (M19, PM at  $m/z$  464.1649, Table 1) was identified by the corresponding aglycone at  $m/z$  384.2087. The PI at  $m/z$  250.1354 and  $m/z$  233.1088 indicated an unaltered 7-azaindole core and 5-fluoropentyl chain, and  $m/z$  135.0807 formed by hydroxylation at the cumyl moiety. The aryl-monohydroxylated/glucuronidated metabolite (M20, PM at  $m/z$  560.2402, Table 1) was identified by the corresponding aglycone at  $m/z$  384.2081, as well as the PI at  $m/z$  135.0805 and  $m/z$  107.0495 representing a hydroxylation at the aryl moiety, and  $m/z$  250.1349 suggesting an unaltered 7-azaindole core and 5-fluoropentyl chain.

The aryl- and 5-fluoropentyl-dihydroxylated/sulfated metabolite (M21, PM at  $m/z$  480.1599, Table 1) was identified by the aglycone at  $m/z$  400.2032, and the PI at  $m/z$  266.1301 and  $m/z$  223.1239 formed by hydroxylation at the 7-azaindole core or 5-fluoropentyl chain. The concurrent presence of  $m/z$  135.0806 indicated a hydroxylation at the cumyl moiety, as well as the PI at  $m/z$  119.0609,  $m/z$  174.0666, and  $m/z$  145.0398 representing an unaltered 7-azaindole core. It was not possible to determine whether sulfation occurred at the aryl- or 5-fluoropentyl hydroxylation, because corresponding fragments without cleavage of the sulfate group could not be detected in the spectra.

In contrast to M21 (Table 1), the aryl-dihydroxylated/sulfated metabolite (M22, PM at  $m/z$  480.1599, Table 1) was identified by the corresponding aglycone at  $m/z$  400.2019. The cleavage of the dihydroxylated cumyl moiety was characterized by the PI at  $m/z$  151.0755 and  $m/z$  123.0443. An unaltered 7-azaindole core was identified by the PI at  $m/z$  174.0662, whereas  $m/z$  250.1350 and  $m/z$  233.1089 characterized an unaltered 5-fluoropentyl chain. The spectra of the formed phase II metabolites differed only in the higher precursor mass, caused by the additional presence of a sulfate or glucuronide, from the corresponding phase I metabolite.

## 3.4 | LC-HRMS/MS fragmentation and identification of cumyl-5F-P7AICA and its *in vivo* phase I and II metabolites using rat and pig urine

### 3.4.1 | Rat urine

In total, eight phase I and two phase II metabolites could be detected (Figure 2) and were found only in low abundances. The major metabolic pathways in rats seemed to be OF/carboxylation, *N*-dealkylation/monohydroxylation/glucuronidation or sulfation, and monohydroxylation, as well as dihydroxylation. The metabolites described later could be found only in rat urine sample. In analogy to the *in vitro* results, the parent compound (PM at  $m/z$  368.2132, Table 1; Figure 1) could also be detected in rat urine.

The *N*-dealkylated/7-azaindole-monohydroxylated metabolite (M11, PM at  $m/z$  296.1393, Table 1; Figure 5B) was identified by the PI at  $m/z$  178.0608,  $m/z$  161.0348, and  $m/z$  135.0553 formed by a hydroxylated 7-azaindole core. In comparison to the unhydroxylated core, there is a mass shift of +16 u of  $m/z$  162.0662 and  $m/z$  119.0606. The *N*-dealkylated/aryl-monohydroxylated metabolite (M12, PM at  $m/z$  296.1393, Table 1; Figure 5C) was identified by  $m/z$  162.0658 and  $m/z$  119.0604, representing an unaltered 7-azaindole core, and the additional presence of  $m/z$  135.0804 formed by a hydroxylated aryl moiety.

The *N*-dealkylated/aryl-monohydroxylated/glucuronidated metabolite (M23, PM at  $m/z$  472.1714, Table 1) was identified by the aglycone at  $m/z$  296.1385. The PI at  $m/z$  135.0800 was formed by a hydroxylated aryl moiety, and the PI at  $m/z$  162.0658 and  $m/z$  119.0608 represented an unaltered 7-azaindole core. The OF carboxamide/carboxylated metabolite (M13, PM at  $m/z$  262.1186, Table 1; Figure S6 [supporting information]) was identified by the PI at  $m/z$

244.1077 and *m/z* 201.1020, indicating the cleavage of the C–O bond of the carboxyl unit, as well as the PI at *m/z* 119.0605 and *m/z* 145.0395, representing an unaltered 7-azaindole core.

### 3.4.2 | Pig urine

In total, one phase I and four phase II metabolites were identified in the analyzed pig urine specimens (Figure 2). The major metabolic pathways of cumyl-5F-P7AICA in pig seemed to be OF/carboxylation, *N*-dealkylation/monohydroxylation/sulfation, and monohydroxylation/glucuronidation or sulfation. The PIs used for the identification of the metabolites (Table 1) were in accordance with those that have already been described in pHS9 incubation results.

In addition, the 5-fluoropentyl-monohydroxylated/glucuronidated metabolite (M24, PM at *m/z* 560.2402, Table 1) could be detected only in pig urine specimens and was identified by the aglycone at *m/z* 384.2092. The PI at *m/z* 119.0860 suggested an unaltered cumyl moiety, *m/z* 266.1302 indicated a hydroxylation at the 7-azaindole core or 5-fluoropentyl chain, and *m/z* 174.0665 represented an unaltered 7-azaindole core.

### 3.5 | CYP initial screening

To elucidate the main metabolic steps in pigs as compared to humans, and the responsible CYP isoenzymes, a CYP activity screening, using human CYP isoenzymes, was performed. All initial steps for cumyl-5F-P7AICA, consisting of *N*-dealkylation, *N*-dealkylation/hydroxylation, OF, OF/carboxylation, ketone formation, monohydroxylation, and dihydroxylation, could be confirmed. As shown in Table 2, cumyl-5F-P7AICA was predominantly metabolized by CYP2C19, CYP3A4, and CYP3A5. The important metabolic steps in pigs and humans, that is, OF followed by carboxylation as well as monohydroxylation, were catalyzed mainly by these three CYP isoenzymes. In addition, *N*-dealkylation, catalyzed by CYP1A2, CYP3A4, and CYP3A5 followed by monohydroxylation through CYP1A2, CYP2C8, CYP2C9, CYP2C19, CYP3A4, and CYP3A5, could

be the main metabolic step in pigs, considering that human CYP isoenzymes were used.

Note. The main metabolizing enzymes are marked in boxes.

Consistent with these findings, the fact that the isoenzymes CYP3A4 and CYP2C19 are involved in the metabolism of SCs, specifically monohydroxylation and dealkylation, has already been demonstrated for different SCs, such as XLR-11, UR-11, AM-2201, RCS-4, and JWH-210.<sup>20,35–37</sup> Oxidative metabolism catalyzed by CYP3A5 could also be observed for several SCs, such as 5F-AKB-48 and EAM-2201.<sup>38</sup>

### 3.6 | Comparison of the metabolic pattern in the different metabolizing systems with human data

#### 3.6.1 | *In vitro* metabolic pattern using pHLM, PLM, and pHS9

The parent compound (Table 3; Figure 1) could be detected in high abundances in all *in vitro* incubation samples. In general, the detected phase I metabolites (Table 3; Figure 2) in the three *in vitro* assays were consistent. The metabolic reactions observed in all three *in vitro* models were OF, OF/carboxylation, OF/aryl-monohydroxylation, *N*-dealkylation, aryl- and 5-fluoropentyl-monohydroxylation, and ketone formation, as well as aryl-dihydroxylation, 5-fluoropentyl-dihydroxylation, and a combination of both. M0 (Table 3; Figure S1 [supporting information]) was detected as an impurity in pHS9, pHLM, and PLM incubations.

In contrast to the results obtained from pHS9 and pHLM incubation samples, OF/5-fluoropentyl-monohydroxylation (M8, Table 3; Figure S4A [supporting information]) could not be identified in PLM incubation. In pHLM, the carboxamide/5-fluoropentyl-monohydroxylated metabolite M9 (PM at *m/z* 266.1299, Table 3; Figure S5 [supporting information]) could not be detected. Due to the fact that M8 (Table 3; Figure S4A [supporting information]) was not found in pig urine as well as in human urine samples, the formation of M8 seems to be species dependent. In addition, M8 (Table 3; Figure S4A [supporting information]) and M9 (Table 3; Figure S5 [supporting information]) were only minor metabolites. Because M0 (Table 3; Figure S1 [supporting information]) could be found

**TABLE 2** Overview of the detected metabolites of cumyl-5F-P7AICA in cytochrome P450 monooxygenase (CYP) initial screening

	CYP										
	1A2	2A6	1B6	2C8	2C9	2C19	2D6	2E1	3A4	3A5	FMO3
<i>N</i> -dealkylation	+								+	+	
<i>N</i> -dealkylation-hydroxylation									+		
Oxidative defluorination (OF)				+	+	+	+			+	
OF-carboxylation						+	+		+	+	
Ketone formation						+			+	+	
Monohydroxylation	+			+	+	+			+	+	
Dihydroxylation						+			+	+	

**TABLE 3** Overview and comparison of cumyl-5F-P7AICA and its phase I and II metabolites detected in different *in vitro* (pooled human liver S9 fraction [pHS9], pooled human liver microsome [pHLM], and pig liver microsome [PLM] incubation) and *in vivo* models (rat urine [RU] after oral administration and pig urine [PU] after inhalative administration) with already-published pHLM incubation<sup>13</sup> and human urine (HU)<sup>11</sup> data

		pHS9	pHLM	PLM	RU	PU	pHLM <sup>13</sup>	HU <sup>11</sup>
	<b>Cumyl-5F-P7AICA</b>	X	x	x	x	x	x	
M0	Carboxamide	X	x	x				
M1	Oxidative defluorinated (OF) and carboxylated	X	x	x	x	x	x	x
M2	Monohydroxylated <sup>1</sup>	X	x	x	x		x	x
M3	Monohydroxylated <sup>2</sup>	X	x	x			x	
M4	Ketone	X	x	x			x	
M5	N-Dealkylated	X	x	x	x		x	
M6	Dihydroxylated <sup>1</sup>	X	x	x			x	
M7	Dihydroxylated <sup>2</sup>	x	x	x	x			
M8	OF-monohydroxylated <sup>2</sup>	x	x					
M9	Carboxamide-monohydroxylated <sup>2</sup>	x		x				
M10	Monohydroxylated <sup>3</sup>	x						x
M11	N-Dealkylated-monohydroxylated <sup>3</sup>				x		x	
M12	N-Dealkylated-monohydroxylated <sup>1</sup>				x			
M13	OF-carboxamide and carboxylated				x			
M14	OF-carboxamide	x						
M15	OF	x	x	x			x	
M16	OF-monohydroxylated <sup>1</sup>	x	x	x			x	
M17	Dihydroxylated <sup>1 + 2</sup>	x	x	x	x		x	
M18	N-Dealkylated-monohydroxylated <sup>1</sup> and sulfated	x			x	x		
M19	Monohydroxylated <sup>1</sup> and sulfated	x				x		x
M20	Monohydroxylated <sup>1</sup> and glucuronidated	x				x		x
M21	Dihydroxylated <sup>1 + 2</sup> and sulfated	x						
M22	Dihydroxylated <sup>1 + 1</sup> and sulfated	x						
M23	N-Dealkylated-monohydroxylated <sup>1</sup> and glucuronidated				x			
M24	Monohydroxylated <sup>2</sup> and glucuronidated					x		

Note. 1, aryl-monohydroxylated; 2, 5-fluoropentyl-monohydroxylated; 3, 7-azaindole-monohydroxylated.

in all *in vitro* samples as an impurity, it is possible that M9 (Table 3; Figure S5 [supporting information]) was formed from M0 (Table 3; Figure S1 [supporting information]) by monohydroxylation at the 5-fluoropentyl chain.

In PLM and pHLM incubations, comparable phase I metabolites were detected. The 7-azaindole-monohydroxylated metabolite (M10, Table 3; Figure 4C) could be detected only in pHS9 incubation samples in low abundances. Due to the presence of the carboxamide linker and the 5-fluoropentyl tail in its chemical structure, steric hindrance could be the reason why monohydroxylation at the 7-azaindole core, resulting in M10 (Table 3; Figure 4C), was seen only in pHS9. In addition, the compound at PM *m/z* 248.1393 (M14, Table 3; Figure S7 [supporting information]) was identified as a carboxamide and OF compound and observed only in pHS9 incubation. As mentioned earlier, this substance could have resulted from the

impurity M0 (Table 3; Figure S1 [supporting information]) with a subsequent phase I reaction.

In addition, phase II reactions, that is, sulfation and glucuronidation of mono- and dihydroxylated as well as N-dealkylated/monohydroxylated compounds, were detected in pHS9 incubation, whereas sulfated compounds were observed more often (Table 3; Figure 2).

In general, the identified phase I metabolic reactions of cumyl-5F-P7AICA in pHLM incubation of the present work were consistent with those published by Staeheli et al,<sup>13</sup> also using pHLM, identifying dihydroxylation, OF/carboxylation, and monohydroxylation as the three major metabolic pathways. In addition, ketone formation (M4, Table 3; Figure S2 [supporting information]), N-dealkylation (M5, Table 3; Figure 5A), OF (M15, Table 3; Figure S8 [supporting information]), and OF/aryl-monohydroxylation (M16, Table 3; Figure S4B

[supporting information]) were observed as metabolic reactions in both pHLM incubations.

In contrast to the already-published data by Staeheli et al.,<sup>13</sup> describing an OF followed by methylation as well as an OF compound in the blank pHLM incubation samples due to the storage of cumyl-5F-P7AICA in methanol, none of those metabolites could be detected as an impurity in the present study. Except for M0 (Table 3; Figure S1 [supporting information]) as an impurity, an OF/5-fluoropentyl-monohydroxylated (M8, Table 3; Figure S4A [supporting information]) and a 5-fluoropentyl-dihydroxylated metabolite (M7, Table 3; Figure S3B [supporting information]) were additionally identified in the present study, but no *N*-dealkylated/monohydroxylated metabolite<sup>13</sup> could be found.

### 3.6.2 | *In vivo* metabolic pattern using rat and pig urine

First, it must be mentioned that the metabolites excreted into rat and pig urine, as well as their abundances, can hardly be compared to each other, as the applied dosages and routes of administrations were different. Nevertheless, if the metabolites detected in rat and pig urine should be compared, it means that, in general, in addition to the parent compound, only a small number of similar phase I and II metabolites were found in rat and pig urine. Although SCs are generally known to be extensively metabolized,<sup>20,39</sup> the excretion of the parent compound into urine has already been reported for other 7-azaindole-derived SCs,<sup>40</sup> as well as, for example, SCs containing an indazole-core structure.<sup>41</sup>

The OF/carboxylated (M1, Table 3; Figure 2) as well as the *N*-dealkylated/aryl-monohydroxylated/sulfated (M18, Table 3; Figure 2) metabolites were detected in high abundances in both rat and pig urine. On the contrary, the metabolites M2, M5, M7, M11, M13, M17, and M23 (Table 3; Figure 2) were detected only in rat urine. In addition, M12 formed by *N*-dealkylation/aryl-monohydroxylation could be found using only this animal model. However, the corresponding phase II metabolites of the aryl-monohydroxylated metabolite (M2) formed by sulfation (M19) or glucuronidation (M20), as well as the 5-fluoropentyl-monohydroxylated/glucuronidated (M24, Table 3) metabolite, could be detected only in pig urine specimens but not in rat urine (Table 3).

The intensive *N*-dealkylation in rats not observed in pig urine samples could be due to differences in CYP isoenzymes.<sup>42</sup> The absence of M2, M7, M12, and M17 (Table 3) in pig urine can be explained by the fact that the monohydroxylated compounds underwent conjugation in pigs, preventing further hydroxylation. This finding is in accordance with results published by Schaefer et al.,<sup>20</sup> describing an intensive phase II metabolism in pigs.

In conclusion, the rat model seems to be less suitable for the elucidation of metabolic patterns of 7-azaindole-containing SCs as compared to the pig model. Due to its highly lipophilic properties, cumyl-5F-P7AICA may not have been sufficiently absorbed after oral administration, thus probably explaining the low abundances of the detected metabolites in rat urine.

### 3.6.3 | Comparison of *in vitro* and *in vivo* metabolism

Comparing *in vitro* and *in vivo* assays, many of the *in vitro* identified phase I metabolites could not be found *in vivo*, except for M1, M2, M5, M7, and M17 (Table 3) also being detected in rat urine. The ketone formation, resulting in M4 (Table 3), as a major metabolic pathway of *in vitro* assays, could not be identified *in vivo*.

Comparing the results of PLM incubation with the elucidated metabolites in pig urine, more phase I metabolites, such as monohydroxylations and dihydroxylations, could be detected. This difference is not surprising, as monohydroxylated compounds undergo conjugation *in vivo*. The metabolites M15 and M16 were identified in PLM but not in pig urine (Table 3). Furthermore, M5 was identified in PLM incubations; however, *N*-dealkylated compounds could not be found in pig urine. A subsequent monohydroxylation of the aryl moiety and conjugation with a sulfate resulting in M18 might be the reason (Table 3).

Based on the high abundances of the formed phase II metabolites *in vivo*, one might conclude that pH9 is more appropriate for the elucidation of the metabolic pattern of 7-azaindole-derived SCs as compared to pHLM and PLM.

### 3.6.4 | Comparison of metabolism in pig with human data

Consistent with the already-published study by Staeheli et al.,<sup>11</sup> phase I and II metabolites detected in pig urine were in good accordance with those found in authentic human urine samples. OF/carboxylation (M1) and aryl-monohydroxylation/sulfation (M19) or glucuronidation (M20) were detected in pig urine as well as in human urine specimens (Table 3) as the main metabolic reactions.

High abundances of the phase I metabolite M1 were observed in pig urine as well as in human urine samples. Regarding this metabolite, no other phase II metabolite could be detected. Therefore, M1 does not appear to be further metabolized by phase II reactions (Table 3). This finding indicates that the intensive formation of an OF/carboxylated metabolite seems to be a major metabolic pathway for cumyl-5F-P7AICA, as already described in a previous study.<sup>11</sup> In addition, this result is consistent with those found for other fluorinated SCs.<sup>43-45</sup>

Furthermore, no dihydroxylated/glucuronidated/sulfated compounds were identified in human and pig urine, which suggests that monohydroxylated compounds undergo a fast phase II conjugation.

On the contrary, some differences between pig and human data were found. To begin with, cumyl-5F-P7AICA was detected in pig urine for 3 h after inhalative administration, but no parent compound could be found in authentic human urine samples by Staeheli et al.<sup>11</sup> (Table 3). As in the casework by Staeheli et al.,<sup>11</sup> nothing is known about the time of consumption as well as the consumed dosage; a consumption of cumyl-5F-P7AICA far before urine sampling may offer an explanation for the fact that no parent compound was found. On the contrary, again in line with our results, the urinary excretion of the



parent compound of 7-azaindole-derived SCs after oral administration was already reported by Giorgetti et al.<sup>40</sup>

M18 and M24 could additionally be detected as phase II metabolites in pig urine but not in human urine (Table 3). This intensive formation of phase II metabolites in pigs is in accordance with already-published metabolism data in pigs by Schaefer et al.<sup>20</sup> This issue could be attributed to species-dependent differences in the formation of these metabolites, because differences in the primary structure of CYP forms, as well as in the gene expression, have already been reported.<sup>42</sup>

On the contrary, the monohydroxylated phase I metabolites M2 and M10 (Table 3) were detected only in studies on human urine performing enzymatic hydrolysis during sample preparation but as mixed spectra.<sup>11</sup> The absence of these metabolites in pig urine samples in our study is not surprising, as no enzymatic hydrolysis was carried out.

In sum, despite minor differences, the metabolic pattern of the *in vivo* pig model was consistent with the already-identified metabolites in human urine samples. In conclusion, the pig is a suitable animal model for the elucidation of recommended urinary targets of 7-azaindole-derived SCs in forensic toxicology.

### 3.7 | Urinary excretion pattern in pig and recommendation of analytical targets

In the present work, the parent compound, cumyl-5F-P7AICA, was detectable in the collected pig urine specimens for 3 h after drug administration, with the abundance decreasing time dependently. Regarding the LC-HRMS/MS data, M20 (Table 3) was the most abundant metabolite for 8 h after administration in our experiment. M19 (Table 3) was also initially predominantly present but disappeared after 7 h. M1 (Table 3; Figure 3), M18 (Table 3), and M24 (Table 3) were found in all collected samples for 8 h but displayed lower abundances.

Assessing the metabolic pattern of other 7-azaindole-derived SCs, such as 5F-MDMB-P7AICA, in pig urine<sup>46</sup>—in contrast to the results obtained in our study of pig—no sulfated phase II metabolites were detected. In addition, the parent compound, 5F-MDMB-P7AICA, was detectable only for 1 h after inhalative administration,<sup>46</sup> whereas in the present study, cumyl-5F-P7AICA could be found for 3 h. This observation could be explained by differences in the chemical structures. Despite an identical 5-fluoropentyl tail, 7-azaindole core, and carboxamide linker, the linked group is different. Whereas cumyl-5F-P7AICA contains a cumyl moiety as a linked group, 5F-MDMB-P7AICA has an ester structure, undergoing a fast degradation due to ester hydrolysis.<sup>46</sup> Regarding indazole-derived SCs, such as 5F-MDMB-PINACA, no parent compound could be detected in urinary specimens;<sup>47,48</sup> however, no systematic controlled studies were conducted.

Based on the aforementioned results and despite the fact that cumyl-5F-P7AICA could not be detected in human urine samples, the parent compound might be a high-specific urinary target to prove the recent consumption of 7-azaindole-derived SCs.

Due to its high abundances in urine samples, M1 (Table 3; Figure 3) might be used as a marker for consumption of cumyl-5F-

P7-AICA, as already described by Staeheli et al.<sup>11</sup> Nevertheless, when interpreting the findings, one must consider that the OF/carboxylated metabolite M1 contains the full parent structure but is not fully specific, because it could also originate by the consumption of, for example, cumyl-5F-PINACA or cumyl-PINACA.<sup>49</sup> Due to the intensive phase II metabolism of cumyl-5F-P7AICA *in vivo*, we further recommend to use the aryl-monohydroxylated/sulfated (M19, Table 3) or glucuronidated (M20, Table 3) metabolites as consumption markers if no enzymatic hydrolysis is performed. To improve the specificity, enzymatic hydrolysis of urine samples could be carried out. In accordance with the study by Staeheli et al, the aryl-monohydroxylated metabolite should also be used as a urinary target to prove consumption, as it includes the full parent structure.<sup>11</sup> This recommendation is confirmed by the fact that monohydroxylation is an already-published common metabolic pathway for SCs.<sup>20,45,50,51</sup>

Due to the high number of structurally similar SCs with common metabolites, high sensitivity and specificity of recommended urinary targets are necessary. To draw a conclusion from the findings of this study and those published by Staeheli et al,<sup>11</sup> urinary targets for the confirmation of a consumption of cumyl-5F-P7AICA should be the parent compound (seemed to be detectable only for a few hours after inhalation), OF/carboxylated as well as the aryl-monohydroxylated metabolite M2 (after enzymatic hydrolysis), and the corresponding sulfated (M19) and glucuronidated (M20) metabolites (Table 3).

## 4 | CONCLUSIONS

The present work elucidated the metabolic patterns of cumyl-5F-P7AICA using different *in vitro* (pHS9, pHLM, and PLM incubations) and *in vivo* (rat and pig) models. In this context, the major metabolic pathways were OF/carboxylation, aryl-monohydroxylation, and aryl-monohydroxylation/glucuronidation or sulfation. CYP2C19, CYP3A4, and CYP3A5 were predominantly involved in the metabolism of cumyl-5F-P7AICA. To prove the consumption of cumyl-5F-P7AICA, the parent compound and the OF/carboxylated, the aryl-monohydroxylated/glucuronidated, or sulfated metabolites should be used as urinary targets. After the enzymatic hydrolysis of urine samples, the aryl-monohydroxylated metabolite might be preferentially used as a urinary marker instead of the glucuronidated or sulfated phase II metabolites. In contrast to the rat model, the pig formed metabolites comparable to those found in human urine specimens except for the parent compound, detected only in pig urine samples for 3 h but not in human urine. Considering all the results of the present study, the pig model is the most suitable animal model for the elucidation of the metabolic pattern of 7-azaindole-derived SCs. In particular, the pig model allows for the elucidation of the time-dependent urinary excretion pattern, because repeated collection of multiple samples is possible.

## ACKNOWLEDGMENTS

We thank the staff of the Institute of Experimental and Clinical Toxicology at Saarland University and the Institute for Clinical and

Experimental Surgery at Saarland University for their support and help during the study. We acknowledge the EU-funded project ADEBAR (IZ25-5793-2016-27).

## ORCID

Nadine Schaefer  <https://orcid.org/0000-0002-5589-9370>

## REFERENCES

- European Monitoring Centre for Drugs and Drug Addiction (EMCDDA). Perspectives on Drugs: Synthetic Cannabinoids in Europe 2017. [www.emcdda.europa.eu/system/files/publications/2753/POD\\_Synthetic%20cannabinoids\\_0.pdf](http://www.emcdda.europa.eu/system/files/publications/2753/POD_Synthetic%20cannabinoids_0.pdf). Accessed April 6, 2020.
- European Monitoring Centre for Drugs and Drug Addiction (EMCDDA). European Drug Report 2018: Trends and Developments. [http://www.emcdda.europa.eu/system/files/publications/8585/20181816\\_TDAT18001ENN\\_PDF.pdf](http://www.emcdda.europa.eu/system/files/publications/8585/20181816_TDAT18001ENN_PDF.pdf). Accessed April 6, 2020.
- Tai S, Fantegrossi WE. Pharmacological and toxicological effects of synthetic cannabinoids and their metabolites. *Curr Top Behav Neurosci*. 2017;32:249-262.
- Karila L, Benyamina A, Blecha L, Cottencin O, Billieux J. The synthetic cannabinoids phenomenon. *Curr Pharm Des*. 2016;22(42):6420-6425.
- Asada A, Doi T, Tagami T, et al. Cannabimimetic activities of cumyl carboxamide-type synthetic cannabinoids. *Forensic Toxicol*. 2018;36(1):170-177.
- Trecki J, Gerona RR, Schwartz MD. Synthetic cannabinoid-related illnesses and deaths. *New Engl J Med*. 2015;373(2):103-107.
- Kraemer M, Boehmer A, Madea B, Maas A. Death cases involving certain new psychoactive substances: a review of the literature. *Forensic Sci Int*. 2019;298:186-267.
- Giorgetti A, Busardò FP, Tittarelli R, Auwärter V, Giorgetti R. Post-mortem toxicology: a systematic review of death cases involving synthetic cannabinoid receptor agonists. *Front Psych*. 2020;11:464-486.
- Darke S, Dufflou J, Farrell M, Peacock A, Lappin J. Characteristics and circumstances of synthetic cannabinoid-related death. *Clin Toxicol (Phila)*. 2020;58(5):368-374.
- Alipour A, Patel PB, Shabbir Z, Gabrielson S. Review of the many faces of synthetic cannabinoid toxicities. *Ment Health Clin*. 2019;9(2):93-99.
- Staheli SN, Steuer AE, Kraemer T. Identification of urinary metabolites of the synthetic cannabinoid 5F-CUMYL-P7AICA in human case-work. *Forensic Sci Int*. 2019;294:76-79.
- Banister SD, Adams A, Kevin RC, et al. Synthesis and pharmacology of new psychoactive substance 5F-CUMYL-P7AICA, a scaffold-hopping analog of synthetic cannabinoid receptor agonists 5F-CUMYL-PICA and 5F-CUMYL-PINACA. *Drug Test Anal*. 2019;11(2):279-291.
- Staheli SN, Poetzsch M, Veloso VP, et al. In vitro metabolism of the synthetic cannabinoids CUMYL-PINACA, 5F-CUMYL-PINACA, CUMYL-4CN-BINACA, 5F-CUMYL-P7AICA and CUMYL-4CN-B7AICA. *Drug Test Anal*. 2018;10(1):148-157.
- Bovens M, Bissig C, Staheli SN, Poetzsch M, Pfeiffer B, Kraemer T. Structural characterization of the new synthetic cannabinoids CUMYL-PINACA, 5F-CUMYL-PINACA, CUMYL-4CN-BINACA, 5F-CUMYL-P7AICA and CUMYL-4CN-B7AICA. *Forensic Sci Int*. 2017;281:98-105.
- Nordmeier F, Richter LHJ, Schmidt PH, Schaefer N, Meyer MR. Studies on the in vitro and in vivo metabolism of the synthetic opioids U-51754, U-47931E, and methoxyacetylfentanyl using hyphenated high-resolution mass spectrometry. *Sci Rep*. 2019;9(1):13774-13791.
- Nordmeier F, Doerr A, Laschke MW, et al. Are pigs a suitable animal model for in vivo metabolism studies of new psychoactive substances? A comparison study using different in vitro/in vivo tools and U-47700 as model drug. *Toxicol Lett*. 2020;329:12-19.
- Richter LHJ, Flockner V, Maurer HH, Meyer MR. Pooled human liver preparations, HepaRG, or HepG2 cell lines for metabolism studies of new psychoactive substances? A study using MDMA, MDBD, butylone, MDPPP, MDPV, MDPB, 5-MAPB, and 5-API as examples. *J Pharm Biomed Anal*. 2017;143:32-42.
- Richter LHJ, Herrmann J, Andreas A, et al. Tools for studying the metabolism of new psychoactive substances for toxicological screening purposes - a comparative study using pooled human liver S9, HepaRG cells, and zebrafish larvae. *Toxicol Lett*. 2019;305:73-80.
- De Brabanter N, Esposito S, Tudela E, et al. In vivo and in vitro metabolism of the synthetic cannabinoid JWH-200. *Rapid Commun Mass Spectrom*. 2013;27(18):2115-2126.
- Schaefer N, Helfer AG, Kettner M, et al. Metabolic patterns of JWH-210, RCS-4, and THC in pig urine elucidated using LC-HR-MS/MS: do they reflect patterns in humans? *Drug Test Anal*. 2017;9(4):613-625.
- Schaefer N, Kettner M, Laschke MW, et al. Distribution of synthetic cannabinoids JWH-210, RCS-4 and  $\Delta^9$ -tetrahydrocannabinol after intravenous administration to pigs. *Curr Neuropharmacol*. 2017;15(5):713-723.
- Schaefer N, Wojtyniak JG, Kettner M, et al. Pharmacokinetics of (synthetic) cannabinoids in pigs and their relevance for clinical and forensic toxicology. *Toxicol Lett*. 2016;253:7-16.
- Swindle MM, Makin A, Herron AJ, Clubb FJ, Frazier KS. Swine as models in biomedical research and toxicology testing. *Vet Pathol*. 2011;49(2):344-356.
- Meurens F, Summerfield A, Nauwynck H, Saif L, Gerdts V. The pig: a model for human infectious diseases. *Trends Microbiol*. 2012;20(1):50-57.
- Anzenbacher P, Soucek P, Anzenbacherová E, et al. Presence and activity of cytochrome P450 isoforms in minipig liver microsomes. *Drug Metab Dispos*. 1998;26(1):56-59.
- Soucek P, Zuber R, Anzenbacherová E, Anzenbacher P, Guengerich FP. Minipig cytochrome P450 3A, 2A and 2C enzymes have similar properties to human analogs. *BMC Pharmacol*. 2001;1(1):11-16.
- Schaefer N, Kroll AK, Korbel C, et al. Distribution of the (synthetic) cannabinoids JWH-210, RCS-4, as well as  $\Delta^9$ -tetrahydrocannabinol following pulmonary administration to pigs. *Arch Toxicol*. 2019;93(8):2211-2218.
- Schaefer N, Wojtyniak JG, Kroell AK, et al. Can toxicokinetics of (synthetic) cannabinoids in pigs after pulmonary administration be upscaled to humans by allometric techniques? *Biochem Pharmacol*. 2018;155:403-418.
- Manier SK, Richter LHJ, Schaper J, Maurer HH, Meyer MR. Different in vitro and in vivo tools for elucidating the human metabolism of alpha-cathinone-derived drugs of abuse. *Drug Test Anal*. 2018;10(7):1119-1130. <https://doi.org/10.1002/dta.2355>
- Wagmann L, Hempel N, Richter LHJ, Brandt SD, Stratford A, Meyer MR. Phenethylamine-derived new psychoactive substances 2C-E-FLY, 2C-EF-FLY, and 2C-T-7-FLY: investigations on their metabolic fate including isoenzyme activities and their toxicological detectability in urine screenings. *Drug Test Anal*. 2019;11(10):1507-1521.
- Meyer MR, Vollmar C, Schwaninger AE, Wolf E, Maurer HH. New cathinone-derived designer drugs 3-bromomethcathinone and 3-fluoromethcathinone: studies on their metabolism in rat urine and human liver microsomes using GC-MS and LC-high-resolution MS and their detectability in urine. *J Mass Spectrom*. 2012;47(2):253-262.
- Michely JA, Helfer AG, Brandt SD, Meyer MR, Maurer HH. Metabolism of the new psychoactive substances N,N-diallyltryptamine (DALT) and 5-methoxy-DALT and their detectability in urine by GC-MS, LC-MSn, and LC-HR-MS-MS. *Anal Bioanal Chem*. 2015;407(25):7831-7842.

33. Caspar AT, Brandt SD, Stoeber AE, Meyer MR, Maurer HH. Metabolic fate and detectability of the new psychoactive substances 2-(4-bromo-2,5-dimethoxyphenyl)-N-[(2-methoxyphenyl)methyl]ethanamine (25B-NBOMe) and 2-(4-chloro-2,5-dimethoxyphenyl)-N-[(2-methoxyphenyl)methyl]ethanamine (25C-NBOMe) in human and rat urine by GC-MS, LC-MS(n), and LC-HR-MS/MS approaches. *J Pharm Biomed Anal.* 2017;134:158-169.
34. EVE and Rave. - The Swiss Drug Forum 2012. <https://www.eve-rave.ch/Forum/viewtopic.php?t=28044>. Accessed April 06, 2020.
35. Holm NB, Nielsen LM, Linnet K. CYP3A4 mediates oxidative metabolism of the synthetic cannabinoid AKB-48. *AAPS J.* 2015;17(5):1237-1245.
36. Stout SM, Cimino NM. Exogenous cannabinoids as substrates, inhibitors, and inducers of human drug metabolizing enzymes: a systematic review. *Drug Metab Rev.* 2014;46(1):86-95.
37. Nielsen LM, Holm NB, Olsen L, Linnet K. Cytochrome P450-mediated metabolism of the synthetic cannabinoids UR-144 and XLR-11. *Drug Test Anal.* 2016;8(8):792-800.
38. Yarbrough AL, Pinson A, Prather PL, et al. Oxidative metabolism and comparative analysis of synthetic cannabinoid N-(1-adamantyl)-1-(5-fluoropentyl)indazole-3-carboxamide (5F-AKB-48) and the unfluorinated analog AKB-48. *FASEB J.* 2019;33(1\_supplement):469.466-469.466.1-1.
39. Mogler L, Halter S, Wilde M, Franz F, Auwärter V. Human phase I metabolism of the novel synthetic cannabinoid 5F-CUMYL-PEGACLONE. *Forensic Toxicol.* 2019;37(1):154-163.
40. Giorgetti A, Mogler L, Haschimi B, et al. Detection and phase I metabolism of the 7-azaindole-derived synthetic cannabinoid 5F-AB-P7AICA including a preliminary pharmacokinetic evaluation. *Drug Test Anal.* 2020;12(1):78-91.
41. Yeter O, Ozturk YE. Metabolic profiling of synthetic cannabinoid 5F-ADB by human liver microsome incubations and urine samples using high-resolution mass spectrometry. *Drug Test Anal.* 2019;11(6):847-858.
42. Turpeinen M, Ghiciuc C, Opritoui M, Tursas L, Pelkonen O, Pasanen M. Predictive value of animal models for human cytochrome P450 (CYP)-mediated metabolism: a comparative study in vitro. *Xenobiotica.* 2007;37(12):1367-1377.
43. Watanabe S, Kuzhiumparambil U, Nguyen MA, Cameron J, Fu S. Metabolic profile of synthetic cannabinoids 5F-PB-22, PB-22, XLR-11 and UR-144 by *Cunninghamella elegans*. *AAPS J.* 2017;19(4):1148-1162.
44. Wohlfarth A, Gandhi AS, Pang S, Zhu M, Scheidweiler KB, Huestis MA. Metabolism of synthetic cannabinoids PB-22 and its 5-fluoro analog, 5F-PB-22, by human hepatocyte incubation and high-resolution mass spectrometry. *Anal Bioanal Chem.* 2014;406(6):1763-1780.
45. Wohlfarth A, Pang S, Zhu M, et al. First metabolic profile of XLR-11, a novel synthetic cannabinoid, obtained by using human hepatocytes and high-resolution mass spectrometry. *Clin Chem.* 2013;59(11):1638-1648.
46. Doerr A, Nordmeier F, Walle N, et al. Can a recently developed pig model be used for in vivo metabolism studies of 7-azaindole derived synthetic cannabinoids? A study using 5F-MDMB-P7AICA as example. *J Anal Toxicol.* 2020. submitted
47. Barceló B, Pichini S, López-Corominas V, et al. Acute intoxication caused by synthetic cannabinoids 5F-ADB and MMB-2201: a case series. *Forensic Sci Int.* 2017;273:e10-e14.
48. McCain KR, Jones JO, Chilbert KT, Patton AL, James LP, Moran JH. Impaired driving associated with the synthetic cannabinoid 5f-Adb. *J Forensic Sci Criminol.* 2018;6(1):105-112.
49. Angerer V, Franz F, Moosmann B, Bisel P, Auwärter V. 5F-Cumyl-PINACA in 'e-liquids' for electronic cigarettes: comprehensive characterization of a new type of synthetic cannabinoid in a trendy product including investigations on the in vitro and in vivo phase I metabolism of 5F-Cumyl-PINACA and its non-fluorinated analog Cumyl-PINACA. *Forensic Toxicol.* 2019;37(1):186-196.
50. Mogler L, Wilde M, Huppertz LM, Weinfurter G, Franz F, Auwärter V. Phase I metabolism of the recently emerged synthetic cannabinoid CUMYL-PEGACLONE and detection in human urine samples. *Drug Test Anal.* 2018;10(5):886-891.
51. Erratico C, Negreira N, Norouzzadeh H, et al. In vitro and in vivo human metabolism of the synthetic cannabinoid AB-CHMINACA. *Drug Test Anal.* 2015;7(10):866-876.

## SUPPORTING INFORMATION

Additional supporting information may be found online in the Supporting Information section at the end of this article.

**How to cite this article:** Walle N, Nordmeier F, Doerr AA, et al. Comparison of *in vitro* and *in vivo* models for the elucidation of metabolic patterns of 7-azaindole-derived synthetic cannabinoids exemplified using cumyl-5F-P7AICA. *Drug Test Anal.* 2021;13:74-90. <https://doi.org/10.1002/dta.2899>